FULL PAPER

Supramolecular Surface Chemistry: Substrate-Independent, Phosphate-Driven Growth of Polyamine-Based Multifunctional Thin Films

*Waldemar A. Marmisollé, Joseba Irigoyen, Danijela Gregurec, Sergio Moya, and Omar Azzaroni**

The ability to engineer surfaces at the supramolecular level by controlled integration of specific chemical units through substrate-independent methodologies represents one of the new paradigms of contemporary materials science. Here, a method is reported to form multifunctional supramolecular coatings through simple dip-coating of substrates in an aqueous solution of polyamine in the presence of phosphate anions. The chemical richness and versatility of polyamines are exploited as phosphate receptors to form thin functional films on a broad variety of substrates, ranging from metal to carbonaceous surfaces. It is shown that the simple derivatization of pendant amino groups of polyallylamine precursors with different chemical groups can endow films with predefined responsiveness or multiple functions—this translates into one-pot and one-step preparation of substrate-adherent films displaying built-in functions. It is believed that the flexibility, speed, and versatility with which this method provides such robust functional films make it very attractive for preparing samples of fundamental and technological interest.

1. Introduction

One of the most fascinating features of nature is its ability to build up highly functional systems from relatively simple molecular building blocks through noncovalent interactions.[1–3] During the past decade, chemists and materials scientists have sought inspiration from biological systems to develop new classes of materials with superior molecular and interfacial functionalities.[4–6] In recent times, bioinspired chemistry rapidly expanded at the frontiers of surface science offering a broader range of perspectives due to the cross-fertilization of supramolecular and interfacial chemistry concepts. One of the most exciting examples of biomimetic surface chemistry is the use of mussel-inspired polydopamine layers developed by Messersmith and co-workers.[7–10] The spontaneous self-polymerization of dopamine leading to the formation of thin, surface-adherent polydopamine films onto a wide variety of substrates marked a profound departure from traditional surface science by introducing a material-independent, surface modification strategy.[11–14] Motivated by the many diverse applications of polydopamine in surface science, we found that other biologically-inspired supramolecular systems could also display analogous functional interfacial properties through alternative chemical pathways. Self-organization of polyamines and phosphate ions constitutes an important example of noncovalent association in numerous biological media. Supramolecular complexes of biogenic polyamines and orthophosphate anions (Pi), known as nuclear aggregates of polyamines (NAPs), are present in many replicating cells.[15] These NAPs interact with DNA phosphate groups and modulate conformation and protection of DNA more efficiently than single polyamines.[16] In vitro aggregation of polyamines in phosphate buffer yields complexes similar to NAPs, which suggest that NAPs are formed spontaneously in cells. H NMR results indicate that spermidine and spermine ammonium forms interact with phosphate anions.[15] Even, changes in the electronic structure of polyamines have been assigned to the interaction with Pi in aggregates.[17] Although electrostatic interactions are probably the main driving force for NAPs formation, hydrogen bonds are also thought to be important for stabilizing the three-dimensional structure.[16] Initial complexes have a cyclic structure and dispose around DNA in tube-like arrangements. They can also be hierarchically stacked to produce macroscopic filamentous structures.[18]

On the other hand, polyamines are known to play a fundamental role in the biogenesis of biosilica in diatoms.[19] Long-chain polyamines and silaffins (proteins with a high degree of polyamines and phosphates as post-translational modifications) represents the main organic components of biosilica and promote specific mineral patterns.[20] These substances induce rapid silica precipitation from silicic acid solution even from

Dr. W. A. Marmisollé, Prof. O. Azzaroni
Instituto de Investigaciones Fisicoquímica Teóricas y Aplicadas (INIFTA)
Departamento de Química
Facultad de Ciencias Exactas
Universidad Nacional de La Plata (UNLP)
CONICET (1900), La Plata, Argentina
E-mail: azzaroni@inifta.unlp.edu.ar
J. Irigoyen, D. Gregurec, Dr. S. Moya
Soft Matter Nanotechnology group
CIC biomaGUNE
Paseo Miramón 182, 20009 San Sebastian, Gipuzkoa Spain

DOI: 10.1002/adfm.201501140

diluted and mild acidic solutions.[21,22] The presence of inorganic phosphate in diatom cell walls suggests that phase separation of polyamines and phosphates takes place during cell wall formation. Phosphate ions induce aggregates of polyamines and highly phosphorylated silaffins and this microscopic phase separations seems to be a prerequisite for in vitro silica precipitation.[21,23] Polyamine/Pi aggregates guide the production of specific silica structures under slightly different conditions. Silica precursors adsorb or dissolve in the polyamine/Pi microphase which determines the final structure.[24] Phosphate aggregation of polyamines is dependent on pH and Pi concentration, and the corresponding changes with pH are reversible. So, this could be a tuning parameter inside diatom vesicles.[21]

Polyallylamine hydrochloride (PAH) has been extensively employed as polyamine model. PAH is known to induce changes in silica formation and structure.[24] It has been reported that the microscopic phase separation of PAH induced by silicic acid is related to its ability to induce silica precipitation.[25] Multivalent anions such as phosphate or sulfate efficiently induce this microscopic phase separation.[25] ^{31}P NMR indicates PAH interactions with phosphate species are present in the pH range where amine groups are protonated ($4 < pH < 9$) but this is not sufficient to induce aggregation and other effects beyond the electrostatic one.[21] The possibility of setting a hydrogen bond network seems to be essential and, in this sense, orthophosphate anion meets the structural geometric requirements and ability to form hydrogen bonds.[21] Pi forms aggregates more efficiently than other divalent anions and it has been suggested the possibility of additional proton dissociation induced by interaction with protonated amines of PAH.[26] The analysis of spinning side bands of ^{31}P NMP indicates that phosphates are mobile in the PAH aggregates compared to solid salts of phosphates. Its mobility is reduced by in vitro silicification, i.e., the same kind of mobility found in diatom cell walls.[21] Pi dimers and trimmers (pyrophosphate and tripolyphosphate anions) are also able to efficiently induce PAH aggregation into colloidal complexes that yield stable macroscopic gels as a precipitate when the concentration is high enough.[27] These macroscopic gels have been also shown to adhere to both hydrophobic and hydrophilic surfaces.[27,28]

On the other hand, specific adsorption of phosphate anions to amino-terminated self-assembled monolayers (SAMs) has been recently proved by electrochemical impedance spectroscopy.[29] According to this, orthophosphate anions bind to surface amino groups partially reversing its charge and allowing the interaction with positive proteins as cytochrome c.[30] Specific interactions of Pi with PAH has also been shown to reverse charge in LbL assemblies.[31] We should also note that hydrogen bonding is omnipresent in these assemblies and consequently this powerful driving force could be exploited to stabilize the interfacial architecture on a great variety of substrates displaying different chemistries, in close resemblance to polydopamine.[11]

Here, we report a new substrate-independent strategy to modify surfaces relying upon the formation of polyamine-phosphate supramolecular complexes. We show that these supramolecular architectures are powerful building blocks for spontaneous deposition of thin polymer films—one-pot surface modification strategy—on virtually any material surface and that the deposited films are compatible with a wide variety of functional uses. We illustrate the method by modifying metal, glass, oxide, plastic, and carbonaceous surfaces with different chemical functionalities. The one-step approach employs simple immersion in mild, dilute aqueous solutions containing both precursors: phosphate and PAH grafted with predefined chemical functions. Stable nanometric films are formed after some minutes in conditions at which no macroscopic precipitation is observed. Depending on chemical or biological functions of groups grafted to PAH backbone; applications such as redox-active surfaces, electroless metallization, and biorecognition are demonstrated.

2. Results and Discussion

The proposed functionalization strategy is represented in **Scheme 1**. Dilute solutions containing the corresponding precursors, polyamine (PAH, 0.2 mg mL^{-1} pH 7 solution) and phosphate (Pi, 10×10^{-3} M pH 7 solution), were mixed together in a beaker in a 1:1 volume ratio. Thereafter, simple immersion of substrates in the aqueous PAH/Pi assembly solution resulted in spontaneous deposition of a thin adherent coating layer. Topographic imaging by atomic force microscopy (AFM) indicated that PAH/Pi supramolecular complexes assembled on cysteamine-modified gold surfaces from solution are evenly distributed on the substrate (**Figure 1**). The film thickness was determined to be 10 nm for this sample, with a RMS roughness of 2.4 nm.

Growth kinetics of PAH/Pi thin films was evaluated by surface plasmon resonance spectroscopy (SPR). **Figure 2**a shows the time evolution of the change in the angle of minimum reflectivity for the SPR scan during the formation of PAH/phosphate coatings on cysteamine-modified Au substrates. Solutions were prepared by mixing pH adjusted PAH and Pi solutions and immediately injected to the SPR cell. After 140 min, the PAH/Pi solution was replaced by fresh buffer and then by pure water. The changes in the minimum angle of the SPR curve indicate the adsorption of material on the amino-terminated surface. Although deposition rates steadily decrease during the period of the experiment, deposition does not reach a plateau even after 140 min. Both the speed as well as the extent of deposition depend on PAH concentration. By using the sensitivity factors of the SPR and the (dn/dc) of 0.16 cm^3 g^{-1} for PAH solutions,[32] the surface coverage of PAH/Pi complexes assembled on the gold substrates were estimated from the SPR minimum angle for two wavelengths, 670 and 785 nm, after extensive washing with water (Figure 2b). Noteworthy, coatings are stable both in buffer solution and in pure water. From the AFM analysis of similar samples, determined by AFM for similar samples, the thickness of the PAH/Pi coatings can be estimated to be 1, 3, 13, and 23 nm for samples prepared from 0.025, 0.05, 0.1, and 0.2 mg mL^{-1} PAH solutions, respectively.

The PAH/Pi film formation and stability were also studied by QCM-D. **Figure 3**a shows the frequency shift during the deposition of PAH/Pi from a PAH solution 0.05 mg mL^{-1} in 5×10^{-3} M pH 7 Pi buffer. According to the frequency shift respect to water, a mass of 3.4 μg cm^{-2} can be obtained by assuming the validity of Sauerbrey equation ($\Delta m = -C\ (\Delta f/n)$,

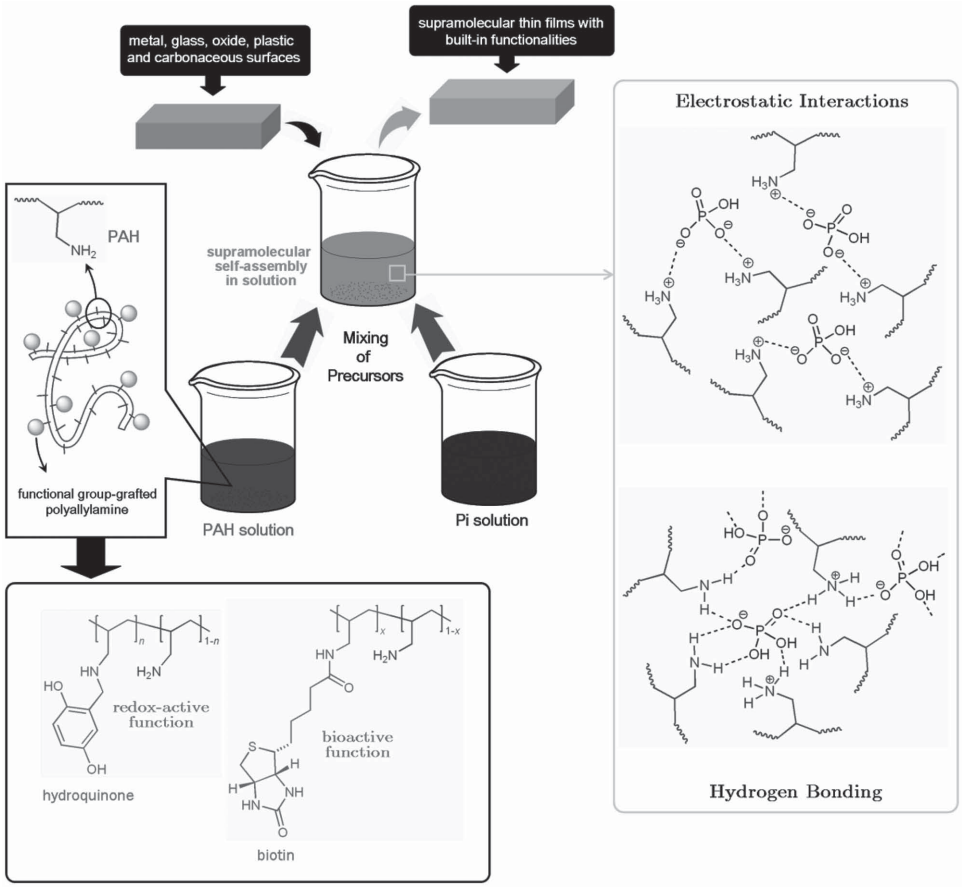

Scheme 1. Representation of the assembly procedure for surface modification with polyamines and phosphate ions (left). The interaction mechanism between PAH and Pi species is also described (right).

with $C = 17.7$ ng cm^{-2} Hz^{-1}). In this case, the value of the ratio $\Delta D/(\Delta f/n) \cong 0.02$ Hz^{-1} and the coincidence of normalized frequency shifts for the analyzed overtones allow applying the Sauerbrey equation. This mass is higher than that obtained by SPR, as it could be expected since QCM is sensitive to the mass of the hydrated film whereas SPR measures the dry mass of the adsorbed material.[33] Results in Figure 3a confirm that the film is stable in both, Pi buffer and water. To evaluate the effect of pH on the stability, successive injections of 5×10^{-3} M Pi solutions of different pH at 500 µL min^{-1} were performed. In Figure 3b we can observe that the film is stable when going from pH 7 to 3. Even a small increase in mass was detected, probably due to the increase in the protonation degree of PAH that requires to bind more anions in compensation. On the other hand, the film was practically removed when exposed to a pH 12 KOH solution. This suggests that treatment with basic solutions could be an affective disassembling method. This pH stability has been reported for macroscopic gels obtained from precipitation of PAH by polyphosphates and dissolution of gels at high pH has been assigned to the deprotonation of PAH drastically reduced its linear charge density.[28] Figure 3c shows the mass changes of cysteamine-modified Au QCM sensors after 80 min of contact with quiescent solutions PAH of several concentrations in 5×10^{-3} M pH 7 Pi. In accordance with SPR measurements, the amount of deposited material depends linearly on PAH concentration. These SPR and QCM results indicate that the amount of material deposited on the substrate can be precisely tuned by selecting the PAH concentration and immersion times. Interestingly, no macroscopic precipitation of the PAH/Pi complexes was observed for the concentrations and times employed in these experiments.

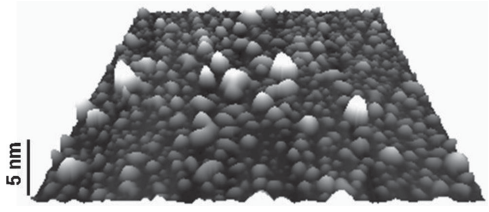

Figure 1. Atomic force microscopy image corresponding to 3D topographic imaging (500 mm × 500 nm) of PAH/Pi supramolecular film complexes assembled on gold surfaces.

The chemical composition of the dried PAH/Pi film was determined by X-ray photoelectron spectroscopy (XPS). **Figure 4** shows N1s and P2p regions of the XPS spectra of a Au/cysteamine substrate modified overnight by immersion in a 0.1 mg mL^{-1} PAH in 5×10^{-3} M pH 7 Pi solution. The binding energy was calibrated to the adventitious carbon at 285 eV (see

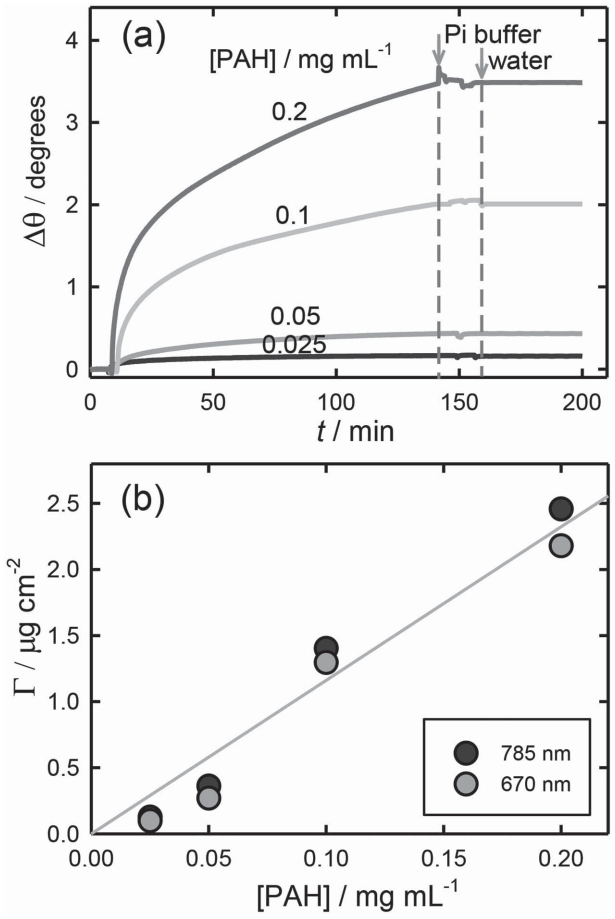

Figure 2. a) Change in the minimum reflectivity angle of the SPR scan (measured at $\lambda = 670$ nm) during the formation of PAH/Pi coatings on cysteamine-modified Au substrates from PAH solutions of different concentration in 5×10^{-3} M pH 7 Pi buffer. b) Dependence of surface coverage on initial PAH bulk concentration.

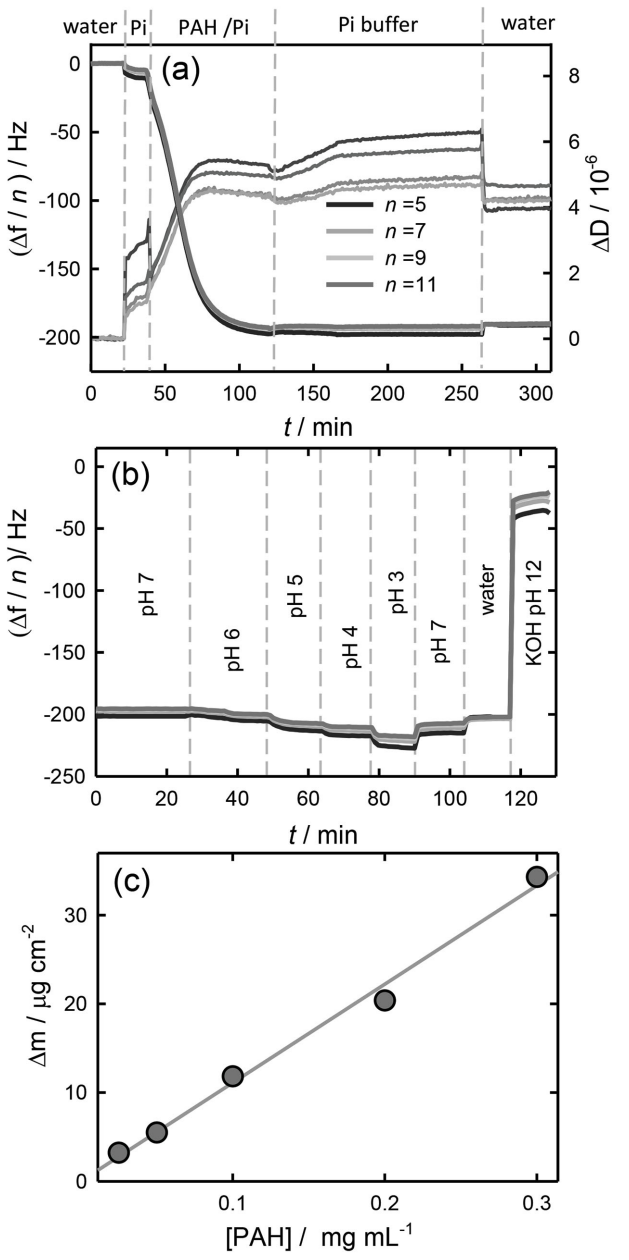

Figure 3. a) Changes in frequency and dissipation during the modification of a cysteamine-coated Au QCM-D sensor with PAH (0.05 mg mL^{-1} in 5×10^{-3} M pH 7 Pi buffer). Flow rate: 160 mL min^{-1}. b) Changes in frequency of the PAH/Pi-coated sensor during the injection of solutions of increasing pH with water washings in between at 500 mL min^{-1}. c) Mass changes after 80 min reaction (assembly) in 5×10^{-3} M pH 7 Pi buffer with increasing concentrations of PAH.

the Supporting Information). The quantitative results of the fittings are summarized in **Table 1**.

N 1s XPS is resolved into two peaks, at binding energies corresponding to 401.2 and 399.3 eV (Figure 4).[34,35] These peaks have been assigned to N–C species of protonated and neutral amines, respectively.[34,36] From the integration of these two contributions, a protonation degree of 0.70 was determined for PAH. This value is consistent with the reported apparent pKa of about 9.2[21] for PAH and the broadening of pKa distribution in polyelectrolytes.[37] P2p region shows the spin orbit coupling with binding energy positions at 133.2 for $P2p_{3/2}$ and 134.0 eV for $P2p_{1/2}$. The atomic N/P ratio was determined to be 2.7. This indicates that more than two amine groups per phosphate anion are present in the coatings. By considering that 70% of the amines are protonated and assuming the aggregates are electrically neutral, the average charge in phosphate species results in 1.86, which is close to the value of 1.6 calculated from the pKa of orthophosphate in solution at pH 7. Finally, the analysis of O1s core level (see the Supporting Information for details) allowed estimating an O/P atomic ratio of 4.4. This value indicates that the main oxygen source is from the Pi, and some minor contribution surely comes from atmospheric contamination (see the Supporting Information for details) and probably from water tightly bound to amine groups as previously reported.[35]

To gain further information on the structure of the PAH/Pi coatings, Fourier transform infrared (FTIR) spectroscopy was performed in the attenuated total reflection (ATR) mode. **Figure 5** shows the ATR-FTIR spectra (2000 to 600 cm^{-1}) of a PAH/Pi film deposited on a cysteamine-modified gold substrate

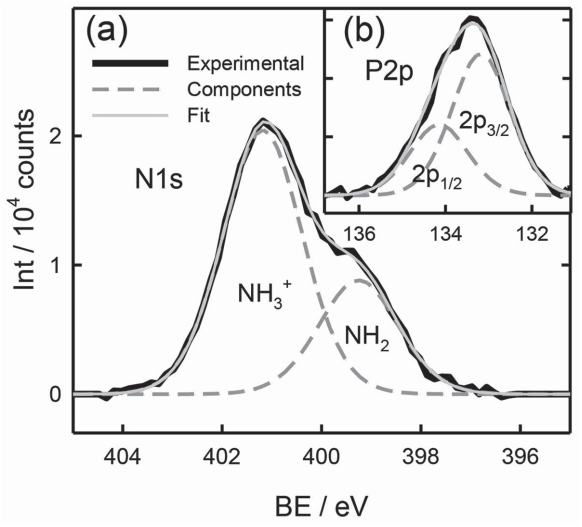

Figure 4. XPS spectra and fittings of a PAH/Pi film in the binding energy region of a) N1s and b) P2p.

and also solid PAH (chloride salt) and solid KH_2PO_4 recorded in the same conditions. For the solid KH_2PO_4 (Figure 5a), the broad IR bands at about 850 and 1050 cm^{-1} has been assigned to phosphate symmetric stretching modes.[38] The band at 1257 cm^{-1} is due to the bending δ(PO—H···O—P) mode and indicates the presence of hydrogen bonds between $H_2PO_4^-$ molecules in the solid.[39] This band is also present when just small clusters of phosphates connected by hydrogen bonds are formed in the initial stages of crystallization.[38] The broad band at about 1600 cm^{-1} has also been assigned to hydrogen bonds formed in the solid, although bending modes of water molecules appear in this region too.[39] The absence of the band at 1257 cm^{-1} in the spectrum of the PAH/Pi film proves that phosphates are not connected between them (as it happens in crystalline KH_2PO_4 and $NH_4H_2PO_4$) but probably interacting with other species in amorphous structures as depicted in Scheme 1. Furthermore, this band is absent when $H_2PO_4^-$ are isolated in aqueous solution and hydrogen bonds are formed with water molecules.[38] In solution, the broad phosphate stretching bands splits into more bands, assigned to both symmetric and asymmetric stretching modes at about 875, 1075, 1150, and 940 cm^{-1}.[39] These bands have been also reported for amorphous $NH_4H_2PO_4$ where the formation of hydrogen bonds between the ammonium and $H_2PO_4^-$ has been proved.[38,39] These peaks are present in the spectrum of PAH/Pi films (Figure 5c). Although, the main peaks in this region can be explained by considering $H_2PO_4^-$ species, the presence of HPO_4^{2-} cannot be discarded as it also shows some peaks in the region 800–1100 cm^{-1} in both solid[40] and aqueous solution.[41]

Table 1. Peak position and assignment of the components employed for fitting XPS results. FWHM in eV are indicated in parentheses.

	Components	
N1s	NH_2	NH_3^+
	399.3 eV (1.9)	401.2 eV (1.9)
P2p	$-PO_4$	
	133.2 eV (2p3/2) (1.6)	134.0 eV (2p1/2) (1.6)

On the other hand, the FTIR spectrum of solid PAH (Figure 5b) shows two main peaks separated by about 100 cm^{-1} in the region 1700–1300 cm^{-1}. These peaks have been assigned to bending modes of protonated amine groups.[42,43] In the present case, they appear at 1494 and 1587 cm^{-1} and correspond to symmetric and antisymmetric bending modes of the protonated primary amines, respectively.[44] There are also two other peaks at about 1450 (here as a shoulder) and 1360 cm^{-1} that has been assigned to CH bending modes.[45] These last two peaks remains practically the same in the PAH/Pi films, but those assigned to ammonium groups shift to higher wavenumbers. This type of shift has also been found when ammonium is adsorbed on negative surfaces,[46] so it could be assigned to the interaction with phosphates.

In order to explore the possible gain of additional functionalities to these coatings, hydroquinone modified PAH (HQ-PAH) was assembled with Pi. Hydroquinone is known to undergo a reversible redox reaction in solution an also when adsorbed on solid substrates.[47] Even more, the dependence of its redox potential on pH has been extensively used for pH measurements.[48] **Figure 6**a shows the voltammetric response of a cysteamine-coated Au electrode modified with HQ-PAH in 5×10^{-3} M pH 7 Pi buffer. All features of the voltammetric response correspond to a quasi-reversible confined redox couple. Peak current linearly increases on sweep rate (Figure 6b) with a slight variation in the peak potential. This indicates the HQ units covalently bound to PAH chains retain their electroactivity in the aggregates and they can be efficiently oxidized and reduced by tuning the electrode potential. Additionally, the electroactivity is pH-responsible as the redox potential (mean potential of the redox peaks) decreases with pH (Figure 6c). The slope of the potential vs pH plot is ≈59 mV, as expected for the HQ couple but it decreases for lower pH. Differences with the pH dependence of HQ redox potential in solution could be related to interactions among redox centers within the coatings[37] and/or Donnan potential drops as found in LbL systems.[49] The higher redox potential of HQ moiety in the coating respect to its value in solution could be attributed to the interaction of the HQ with the polymer or phosphate species in the film. Similar positive shifts in the redox potential have been reported for adsorbed proteins on positive surfaces.[50,51] This supports the idea that it is thermodynamically easier to reduce redox centers (to transfer electrons to them) when they are close to positive charges.

So far, we have explored the assembly of PAH/Pi complexes on model surfaces bearing NH_2 groups.

We should consider that hydrogen bonding is one of the interactions governing the formation of PAH/Pi complexes and consequently, in close resemblance to polydopamine anchoring chemistry, this powerful driving force could be exploited to assemble these functional supramolecular entities on a great variety of substrates prone to form hydrogen bonds, even though they display different chemistries. This conceptual framework was put into practice by assembling HQ-PAH/Pi assemblies on bare graphite electrodes. Carbonaceous surfaces are extremely valuable substrates in many branches of

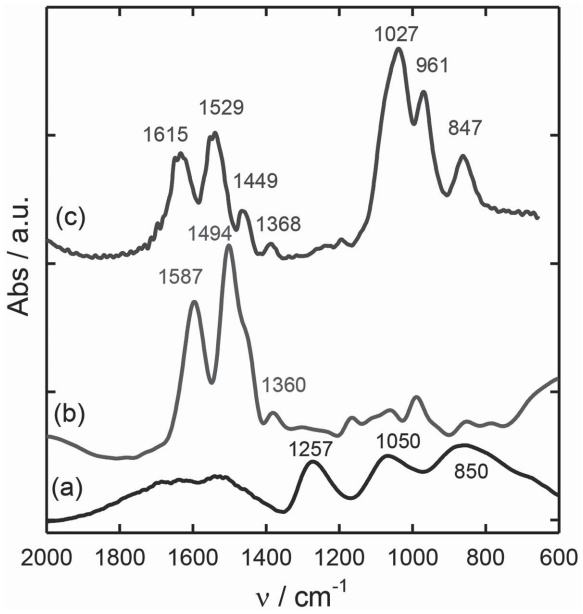

Figure 5. a) ATR-FTIR spectra of solid KH_2PO_4, b) solid PAH, and c) a PAH/Pi film on Au/cysteamine. The position of main peaks in each spectrum is indicated in the figure.

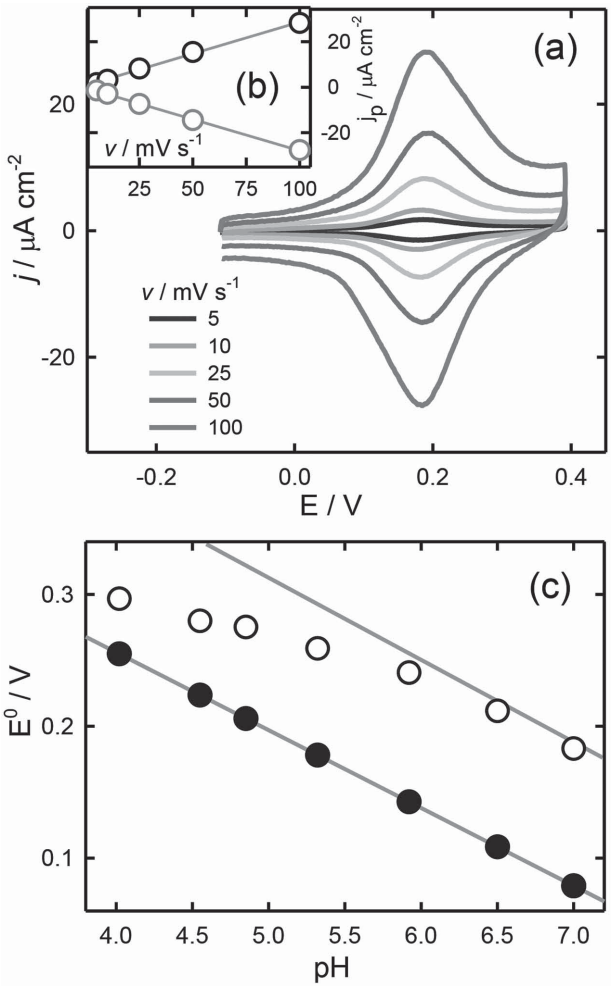

Figure 6. a) Voltammetric response of HQ-PAH/Pi on a cysteamine-coated Au electrode at different sweep rates. b) Dependence of the peak current density on the sweep rate. c) Dependence of the formal redox potential of HQ-PAH/Pi coated electrode on pH (empty circles). Solid circles correspond to calculated value for HQ in solution.

electrochemistry. As is well-known, most of carbonaceous materials are partially oxidized on their surfaces and have a tendency to form strong hydrogen bonds with different species.[52] **Figure 7**a shows cyclic voltammograms of HQ-PAH/Pi layers straightforwardly assembled on bare graphite electrodes. In this case, the graphite electrode has a noticeable double-layer capacitive current. Nevertheless, the baseline corrected electrochemical signal (Figure 7b) clearly indicates that the assembled layer is stable and able to transfer electrons from the hydroquinone groups to the carbon surface. The dependence of the peak current on the sweep rate indicates a layer confined redox couple (Figure 7c). Compared with the cysteamine-coated Au electrode, the electron transfer is slower on the graphite electrode, as indicated by the peak potential shifts in panel (Figure 7b).

The very possibility of addressing the supramolecular assembly of PAH/Pi complexes on surfaces via hydrogen bonding forces opens the door to the functionalization of a broad variety of substrates that are susceptible to these interactions. For example, oxygen sites of oxide surfaces can act as anchoring points to immobilize PAH/Pi assemblies. Following this line of reasoning, we derivatized indium-tin oxide (ITO) electrodes with electroactive hydroquinone groups by direct immersion of the substrates in HQ-PAH/Pi solutions. **Figure 8** displays the electrochemical response of HQ-PAH/Pi complex layers on ITO, thus confirming the successful modification of the conducting oxide surface. In this case, the voltammetric waves are broader and can be better appreciated by subtracting the response of the unmodified electrode in the same conditions.

The same concept was also extended to plastic foils constituted of poly(ethylene terephthalate) (PET). The presence of amino groups in the PAH/Pi film can be used to adsorb some interesting metal complexes. This is the case of $PdCl_4^{2-}$, which has been shown to be an efficient catalyst for Cu electroless deposition.[53,54] PET foils were first modified with PAH/Pi coatings and then immersed in a 1 mM $PdCl_4^{2-}$ solution for 30 min and finally soaked overnight in a Cu electroless bath (**Figure 9**). The adsorbed $PdCl_4^{2-}$ anions are reduced to Pd nanoparticles in the electroless solution and then they induce the Cu deposition. Due to the anchoring of the catalyst to the PAH/Pi film, the Cu coating is tightly bound to the surface allowing the manipulation of the metalized foils without any evidence of delamination (Figure 9c). No Cu deposition was observed on PET foils when the PAH/Pi modification step was omitted.

On the other hand, with the aim of conferring biorecognition properties to the supramolecular films, PAH was functionalized with biotin (b-PAH). Biotin is known to efficiently bind streptavidin and this pair has been extensively employed in molecular recognition-based devices.[55–58] **Figure 10** shows SPR minimum angle changes at two laser wavelengths during modification of a Au/cysteamine sensor with b-PAH and subsequent binding of streptavidin. As indicated by these SPR results, biotin moieties are able to interact with streptavidin

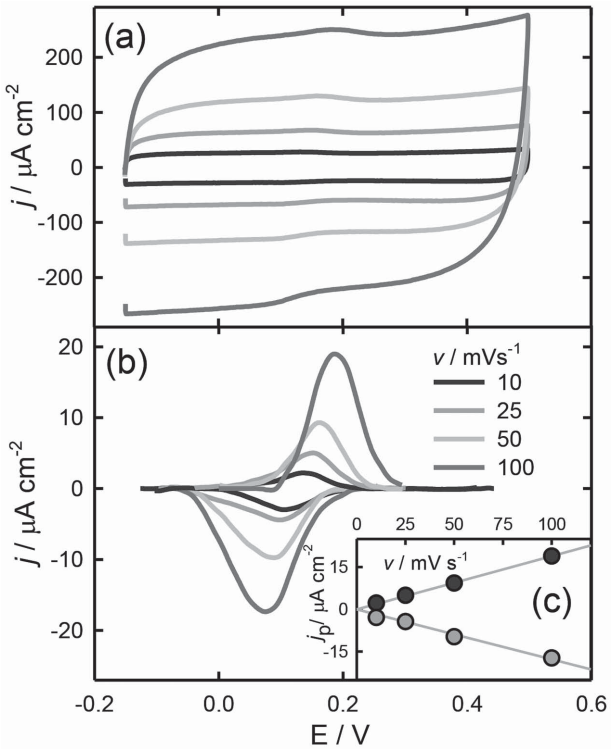

Figure 7. a) Voltammetric response of HQ-PAH/Pi graphite modified electrode at different sweep rates in 5×10^{-3} M pH 7 Pi buffer. b) Baseline corrected peaks. c) Dependence of the peak current density on the sweep rate.

molecules in the PAH/Pi coatings. By using the factors for our SPR and the dn/dc of 0.182 cm^3 g^{-1} for globular proteins, the mean surface concentration results 9.4 pmol cm^{-2}.

These results reveal that biorecognizable elements can be integrated into the film via a one-step method. It is interesting to note that obtained films closely resemble those prepared by the so-called "layer-by-layer" assembly of polyelectrolytes, provided that in both cases the resulting film is constituted of complexed polyelectrolyte chains.[59–61] However, in the case of

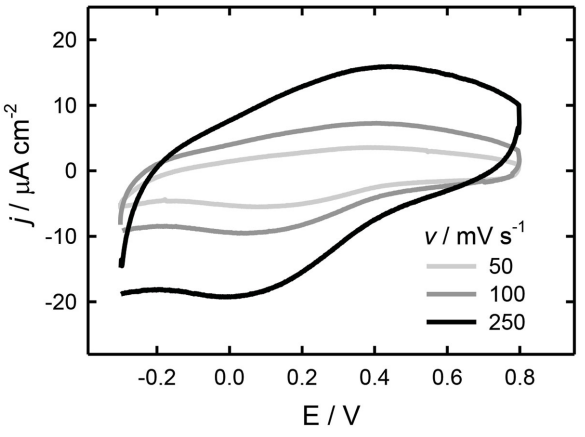

Figure 8. Voltammetric response of HQ-PAH/Pi on ITO in 5×10^{-3} M pH 7 Pi buffer. The background from the unmodified electrode has been removed.

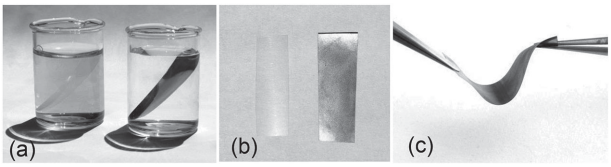

Figure 9. a) PET (left) and PAH/Pi-modified PET (right) foils immersed in the electroless solution after overnight incubation. b) Unmodified and Cu-coated PET foils. c) Twisted Cu-coated PET foil.

the present approach films are generated through a one-pot, one step strategy whereas in LbL assemblies, even though the strategy is very simple, the construction of the film requires sequential assembly of the multiple building blocks, which can be greatly time consuming.

3. Conclusions

In summary, we have presented a simple strategy of surface modification that can be applied to the surface of many diverse materials. By employing this one-step technique, we were able to introduce different functions on various substrates, including metal, oxide, plastic, and carbonaceous surfaces. Our studies demonstrate that PAH-Pi supramolecular complexes displaying built-in functions can be effectively immobilized onto diverse surfaces without the requirement of further time-consuming chemical protocols. The flexibility, speed, and affordability with which this method provides such functional films make it extraordinarily attractive for preparing samples of fundamental and technological interest. More pertinently, the examples presented herein have illustrated the richness and potential of anion coordination chemistry in the presence of polyamine receptors as a key enabling technology to achieve a large variety of multifunctional surfaces regardless of the chemical nature of the substrate. We believe that these results can lead to a new way of looking at supramolecular materials

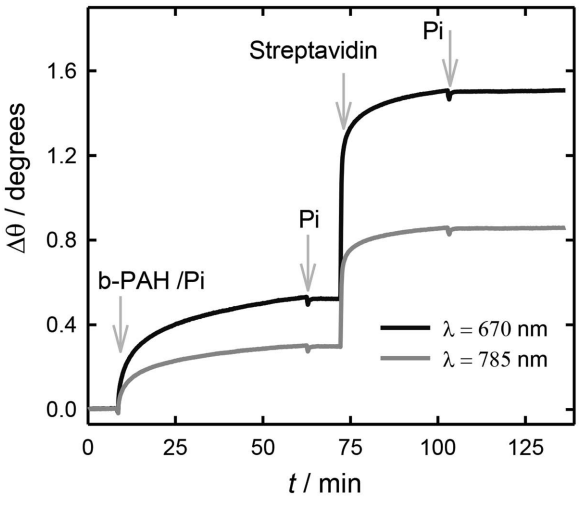

Figure 10. Change in the minimum reflectivity angle of the SPR scan during the formation of biotin-PAH (0.1 mg mL^{-1})/phosphate (5×10^{-3} M Pi pH 7) coating on a cysteamine-modified Au substrate and further assembly of streptavidin (1.1×10^{-6} M in 5×10^{-3} M Pi buffer).

science and trigger a cascade of new, refreshing ideas in supramolecular surface chemistry aimed at the rational design of functional assemblies with tailored properties.

4. Experimental Section

Chemicals: Polyallylamine hydrochloride (≈58 kDa) and cysteamine hydrochloride were purchased from Sigma-Aldrich. KH_2PO_4 was from Carlo Erba. Streptavidin (60 kDa) was from Serva. The pH of stock solutions of PAH (1 mg mL^{-1}) and Pi (10×10^{-3} M KH_2PO_4) was adjusted to 7 by adding 10% KOH. All chemicals were of analytical grade. The water used in all experiments was purified by a Millipore system and its resistivity was 18.2 MΩ cm.

Synthesis of Hydroquinone-PAH: 2,5-Dihydroxybenzaldehyde (12 mg) was dissolved in 5 mL of methanol and added dropwise within an hour to 30 mL of anhydrous methanolic solution of 40 mg of poly(allylamine) containing 0.20 mL of triethylamine. The mixture was stirred for another hour at room temperature, sodium borohydride was carefully added in portions at 0 °C, and stirring continued for 90 min; finally the mixture was dried in vacuo at 35 °C. The residue of hydroquinone-PAH (HQ-PAH) was extracted with distilled water. The aqueous solution was further purified by membrane dialysis against water. [62] The content of hydroquinone was determined by ^{1}H NMR and was found to be 15%.

Synthesis of Biotin-PAH: 6-Biotinyl-*N*-hydroxysuccinimide ester (0.41 g, 1.26×10^{-3} mol) was dissolved in 3 mL of DMF by heating to 80 °C.[63] The solution was cooled to room temperature and was added dropwise to a solution of 0.5 g of PAH (15 kDa) solution in 3 mL of aqueous Tris buffer containing 0.13 g of $NaHCO_3$ (1.575×10^{-3} mol, 1.5 equiv of biotin-NHS. The clear solution obtained was allowed to stir at room temperature for 24 h and was subjected to dialysis against water for 5 d (dialysis membrane cutoff was 3500). The aqueous solution was lyophilized to give biotinylated poly(allylamine) hydrochloride (b-PAH) as a white solid. The content of biotin was determined by ^{1}H NMR and was found to be 21%.[64]

Copper Electroless Deposition: PET foils were cleaned by sonication in water, ethanol, 6 M NaOH and water again for 15 min each. Clean PET foils were modified by immersion in 0.1 mg mL^{-1} PAH in 5×10^{-3} M pH 7 Pi buffer for 60 min. They were then washed with 5×10^{-3} M Pi buffer and immersed in 1×10^{-3} M $PdCl_4^{2-}$ in HCl (pH 2) for 30 min. After washing with Pi buffer, the modified plates were immersed in the electroless solution overnight. The electroless solution was a mixture 1:1 of Solution A and Solution B. Solution A: 12 g L^{-1} NaOH (Biopack) + 13 g L^{-1} $CuSO_4 \cdot 5H_2O$ (Biopack) + 29 g L^{-1} $KNaC_4H_4O_6 \cdot H_2O$ (Anedra). Solution B: 20 mL L^{-1} formaldehyde (Dorwil).[53]

Cysteamine SAM Preparation: For cysteamine modification, Au substrates were tipically soaked overnight in 2×10^{-3} M cysteamine in acid ethanolic solution (4:1 v/v C_2H_5OH–$HClO_4$ 10^{-4} M pH = 4) to prevent binding through the NH_2 groups.[29] Then substrates were thoroughly rinsed with ethanol and water and dried under a stream of nitrogen gas.

Atomic Force Microscopy: The substrate employed for AFM measurements was a glass slide coated with ≈100 nm of Au on a thin layer of Ti used as mordant. The Au surface was modified with a SAM of cysteamine as just described.The modified substrate was incubated in 0.1 mg mL^{-1} PAH in 5×10^{-3} M pH 7 Pi buffer for 60 min. A Veeco Multimode AFM connected to a Nanoscope V controller was used to image the substrate. AFM measurements were performed in tapping mode in a closed fluid cell filled with 5×10^{-3} M pH 7 Pi solution using a DNP-S10 (Bruker, K = 0.32 N m^{-1}) cantilever.

Surface Plasmon Resonance Spectroscopy: Gold sensors (glass slides coated with ≈48 nm of gold and ≈2 nm of chromium, BioNavis Ltd, Tampere, Finland) were employed for SPR measurements. These substrates exhibit a refractive index (RI) of 1.5202 at 670 nm. SPR sensors were cleaned by immersion in boiling NH_4OH (28%)/H_2O_2 (100 vol) 1:1 for 15 min and then rinsed with water and ethanol. Then, they were modified with a cysteamine SAM. Multi-Parametric Surface Plasmon Resonance (MP-SPR) experiments were carried out using a SPR Navi 210A instrument (BioNavis Ltd, Tampere, Finland). An electrochemistry flow cell (SPR321-EC, BioNavis Ltd.) was employed for all measurements. Injection was performed manually and SPR angular scans (two wavelength mode) were recorded with no flow in the cell. Temperature was kept at 20 °C. All SPR experiments were processed using the BioNavis Data viewer software.

Quartz Crystal Microbalance (QCM) and Quartz Crystal Microbalance with Dissipation (QCM-D): QCM measurements were performed with a QCM200 Quartz Cristal Microbalance supplied with Gold QCM25 5 MHz oscillators (Sensitivity factor: 56.6 Hz cm^2 μg^{-1}) (Stanford Research Systems). Gold oscillators were modified with cysteamine as described previously. Determinations were performed with quiescent solutions in a Teflon cell at 23 °C. QCM-D experiments were performed using a Q-Sense instrument (QCM-D, Q-Sense E4) equipped with a flow module. Samples are perfused using a peristaltic microflow system. Measurements were recorded at several odd overtones and frequency shifts were normalized taking into account the overtone number (n). All experiments were performed at 23 °C. A QSX 301 5 MHz gold sensor was employed. In this case, the gold sensor was modified with the thiol in situ by allowing a 2×10^{-3} M cysteamine ethanolic solution to flow at 100 μL min^{-1} for 30 min. Successive injections of ethanol and water at 500 μL min^{-1} for 5 min were employed for removing the thiol not bound.

X-Ray Photoelectron Spectroscopy): X-ray photoelectron spectroscopy was performed using a SPECS SAGE HR 100 system spectrometer. A Mg Kα (1253.6 eV) X-ray source was employed operating at 12.5 kV and 10 mA. Survey spectra were obtained with pass energy of 30 eV whereas 15 eV was employed for detailed spectra of C1s, O1s, N1s, and P2p regions. The take-off angle was 90° and operating pressure was 8×10^{-8} mbar. Under this condition, BE resolution was determined to be 1.1 eV. Quantitative analysis of spectra was carried out with the Casa XPS 2.3. 16 PR 1.6 software. Shirley baselines and Gaussian\Lorentzian (30%) product functions were employed. To compensate surface-charging effects, the binding energy (BE) of the aliphatic core level C1s was set at 285 eV. The full width at half maximum (FWHM), was kept fixed for different components of a given element. Survey atomic ratios were calculated from the integrated intensities of core levels after instrumental and photoionization cross section correction. For N/P and O/P, more precise calculations were performed by recording the XPS spectrum $(NH_4)_3PO_4$ (Sigma-Aldrich) powder in the same conditions as internal reference.

FTIR Spectroscopy: Fourier transform infrared spectroscopy in the attenuated total reflection mode was performed using a Varian 600 FTIR spectrometer equipped with a ZnSe ATR crystal with a resolution of 1 cm^{-1}. Background-subtracted spectra were corrected for ATR acquisition by assuming a refractive index of 1.45 for all of the samples.

Cyclic Voltammetry: Measurements on cysteamine-modified gold were performed in the SPR cell where the gold sensor was the working electrode. Cyclic voltammetry (CV) was performed using a Gamry REF600 potentiostat. A Pt wire was employed as counter electrode and a AgCl coated silver wire was employed as pseudo-reference electrode. Its potential was measured against a true Ag/AgCl (3 M NaCl) reference electrode in buffer solution after SPR measurements. Potentials reported here are referred to this electrode. Measurements on graphite (3 mm diameter rod, Aldrich) and ITO (Delta Technologies) were performed in a conventional three electrodes electrochemical cell. A Teq-03 potentiostat (TEQ, Argentina) was employed. The counter electrode was a Pt wire and a Ag/AgCl (3 M NaCl) electrode was employed as reference. The clean substrates were first potential cycled in 5×10^{-3} M pH 7 Pi buffer until a stable response was obtained. Then they were immersed for 60 min in fresh 0.1 mg mL^{-1} HQ-PAH solution in 5×10^{-3} M pH 7 Pi buffer. After that, they were rinsed with Pi buffer and water prior to the electrochemical measurements.

Acknowledgements

This work was financially supported by the Marie Curie project "Higraphen Hierarchical functionalization and assembly of graphene for multiple device fabrication" (HiGRAPHEN) (Grant No. 612704),

Consejo Nacional de Investigaciones Científicas y Técnicas (CONICET – Argentina), Agencia Nacional de Promoción Científica y Tecnológica (ANPCyT – Argentina; PICT-163/08, PICT-2010–2554, PICT-2013–0905), the Austrian Institute of Technology GmbH (AIT–CONICET Partner Group: "Exploratory Research for Advanced Technologies in Supramolecular Materials Science" – Exp. 4947/11, Res. No. 3911, 28–12–2011), and Universidad Nacional de La Plata (UNLP). W.A.M. and O.A. are staff members of CONICET.

Received: March 20, 2015
Revised: April 23, 2015
Published online: May 21, 2015

[1] *Manipulation of Nanoscale Materials: An Introduction to Nanoarchitectonics* (Ed: K. Ariga), Royal Society of Chemistry, Cambridge **2012**.
[2] *Hydrogen Bonded Supramolecular Materials* (Eds: Z.-T. Li, L.-Z. Wu), Springer-Verlag, Heidelberg **2015**.
[3] J. Simon, P. Bassoul, *Design of Molecular Materials: Supramolecular Engineering*John Wiley & Sons, Chichester **2000**.
[4] J. Li, Q. He, X. Yan, *Molecular Assembly of Biomimetic Systems*Wiley-VCH, Weinheim **2011**.
[5] L. Jiang, L. Feng, *Bioinspired Intelligent Nanostructured Interfacial Materials* Vol. *38*, World Scientific Publishing Company, Singapore **2010**.
[6] C. S. S. R. Kumar, *Biomimetic and Bioinspired Nanomaterials* VCH-Wiley, Weinheim **2010**.
[7] H. Lee, S. M. Dellatore, W. M. Miller, P. B. Messersmith, *Science* **2007**, *318*, 426.
[8] H. Lee, Y. Lee, A. R. Statz, J. Rho, T. G. Park, P. B. Messersmith, *Adv. Mater.* **2008**, *20*, 1619.
[9] H. Lee, J. Rho, P. B. Messersmith, *Adv. Mater.* **2009**, *21*, 431.
[10] S. M. Kang, N. S. Hwang, J. Yeom, S. Y. Park, P. B. Messersmith, I. S. Choi, R. Langer, D. G. Anderson, H. Lee, *Adv. Funct. Mater.* **2012**, *22*, 2949.
[11] Q. Ye, F. Zhou, W. Liu, *Chem. Soc. Rev.* **2011**, *40*, 4244.
[12] J. Sedó, J. Saiz-Poseu, F. Busqué, D. Ruiz-Molina, *Adv. Mater.* **2013**, *25*, 653.
[13] B. P. Lee, P. B. Messersmith, J. N. Israelachvili, J. H. Waite, *Annu. Rev. Mater. Res.* **2011**, *41*, 99.
[14] Y. Liu, K. Ai, L. Lu, *Chem. Rev.* **2014**, *114*, 5057.
[15] L. D'Agostino, A. Di Luccia, *Eur. J. Biochem.* **2002**, *269*, 4317.
[16] L. D'Agostino, M. di Pietro, A. Di Luccia, *FEBS J.* **2005**, *272*, 3777.
[17] A. Di Luccia, G. Picariello, G. Iacomino, A. Formisano, L. Paduano, L. D'Agostino, *FEBS J.* **2009**, *276*, 2324.
[18] G. Iacomino, G. Picariello, F. Sbrana, A. Di Luccia, R. Raiteri, L. D'Agostino, *Biomacromolecules* **2011**, *12*, 1178.
[19] N. Kröger, S. Lorenz, E. Brunner, M. Sumper, *Science* **2002**, *298*, 584.
[20] N. Kröger, R. Deutzmann, C. Bergsdorf, M. Sumper, *Proc. Natl. Acad. Sci. U.S.A.* **2000**, *97*, 14133.
[21] K. Lutz, C. Gröger, M. Sumper, E. Brunner, *Phys. Chem. Chem. Phys.* **2005**, *7*, 2812.
[22] M. Sumper, S. Lorenz, E. Brunner, *Angew. Chem. Int. Ed.* **2003**, *42*, 5192.
[23] M. Sumper, N. Kro, D. Regensburg, *J. Mater. Chem.* **2004**, *14*, 2059.
[24] M. Sumper, *Angew. Chem. Int. Ed.* **2004**, *43*, 2251.
[25] E. Brunner, K. Lutz, M. Sumper, *Phys. Chem. Chem. Phys.* **2004**, *6*, 854.
[26] W. J. Dressick, K. J. Wahl, N. D. Bassim, R. M. Stroud, D. Y. Petrovykh, *Langmuir* **2012**, *28*, 15831.
[27] Y. Huang, P. G. Lawrence, Y. Lapitsky, *Langmuir* **2014**, *30*, 7771.
[28] P. G. Lawrence, Y. Lapitsky, *Langmuir* **2015**, *31*, 1564.
[29] W. A. Marmisolle, D. A. Capdevila, E. De Llave, F. J. Williams, D. H. Murgida, *Langmuir* **2013**, *29*, 5351.
[30] D. A. Capdevila, W. A. Marmisollé, F. J. Williams, D. H. Murgida, *Phys. Chem. Chem. Phys.* **2013**, *15*, 5386.
[31] J. Irigoyen, S. E. Moya, J. J. Iturri, I. Llarena, O. Azzaroni, E. Donath, *Langmuir* **2009**, *25*, 3374.
[32] M. Eriksson, S. M. Notley, L. Wågberg, *J. Colloid Interface Sci.* **2005**, *292*, 38.
[33] E. Reimhult, C. Larsson, B. Kasemo, F. Höök, *Anal. Chem.* **2004**, *76*, 7211.
[34] X. Song, Y. Ma, C. Wang, P. M. Dietrich, W. E. S. Unger, Y. Luo, *J. Phys. Chem. C* **2012**, *116*, 12649.
[35] J. E. Baio, T. Weidner, J. Brison, D. J. Graham, L. J. Gamble, D. G. Castner, *J. Electron. Spectrosc. Relat. Phenom.* **2009**, *172*, 2.
[36] N. Graf, E. Yegen, T. Gross, A. Lippitz, W. Weigel, S. Krakert, A. Terfort, W. E. S. Unger, *Surf. Sci.* **2009**, *603*, 2849.
[37] W. A. Marmisollé, M. I. Florit, D. Posadas, *J. Electroanal. Chem.* **2013**, *707*, 43.
[38] C. Sun, D. Xue, *J. Mol. Struct.* **2014**, *1059*, 338.
[39] C. Sun, D. Xue, *J. Phys. Chem. C* **2014**, *118*, 16043.
[40] T. Mhiri, F. Romain, A. Hadrich, A. Lautie, *Vib. Spectrosc.* **2001**, *26*, 51.
[41] E. J. Elzinga, D. L. Sparks, *J. Colloid Interface Sci.* **2007**, *308*, 53.
[42] D. K. Kim, S. W. Han, C. H. Kim, J. D. Hong, K. Kim, *Thin Solid Films* **1999**, *350*, 153.
[43] J. Choi, M. F. Rubner, *Macromolecules* **2005**, *38*, 116.
[44] G. Lawrie, I. Keen, B. Drew, A. Chandler-Temple, L. Rintoul, P. Fredericks, L. Grøndahl, *Biomacromolecules* **2007**, *8*, 2533.
[45] V. Zucolotto, M. Ferreira, M. R. Cordeiro, C. J. L. Constantino, D. T. Balogh, A. R. Zanatta, W. C. Moreira, O. N. Oliveira, *J. Phys. Chem. B* **2003**, *107*, 3733.
[46] R. A. Rajadhyaksha, H. Knözinger, *Appl. Catal.* **1989**, *51*, 81.
[47] M. Rafiee, D. Nematollahi, *Electroanalysis* **2007**, *19*, 1382.
[48] M. M. Walczak, D. A. Dryer, D. D. Jacobson, M. G. Foss, N. T. Flynn, *J. Chem. Educ.* **1997**, *74*, 1195.
[49] E. J. Calvo, A. Wolosiuk, *J. Am. Chem. Soc.* **2002**, *124*, 8490.
[50] D. A. Capdevila, W. A. Marmisolle, F. Tomasina, V. Demicheli, M. Portela, R. Radi, D. H. Murgida, *Chem. Sci.* **2015**, *6*, 705.
[51] X. Chen, R. Ferrigno, J. Yang, G. M. Whitesides, *Langmuir* **2002**, *18*, 7009.
[52] *Tribology of Diamond-like Carbon Films: Fundamentals and Applications* (Eds: C. Donnet, A. Erdemir), Springer-Verlag, New York **2010**.
[53] O. Azzaroni, Z. Zheng, Z. Yang, W. T. S. Huck, *Langmuir* **2006**, *22*, 6730.
[54] X. Liu, X. Zhou, Y. Li, Z. Zheng, *Chem. - Asian J.* **2012**, *7*, 862.
[55] C. E. Jordan, A. G. Frutos, A. J. Thiel, R. M. Corn, *Anal. Chem.* **1997**, *69*, 4939.
[56] W. Knoll, M. Zizlsperger, T. Liebermann, S. Arnold, A. Badia, M. Liley, D. Piscevic, F.-J. Schmitt, J. Spinke, *Colloids Surf., A* **2000**, *161*, 115.
[57] O. Azzaroni, M. Álvarez, M. Mir, B. Yameen, W. Knoll, *J. Phys. Chem. C* **2008**, *112*, 15850.
[58] M. Ali, B. Yameen, R. Neumann, W. Ensinger, W. Knoll, O. Azzaroni, *J. Am. Chem. Soc.* **2008**, *130*, 16351.
[59] K. Ariga, J. P. Hill, Q. Ji, *Phys. Chem. Chem. Phys.* **2007**, *9*, 2319.
[60] K. Ariga, Y. Yamauchi, G. Rydzek, Q. Ji, Y. Yonamine, K. C.-W. Wu, J. P. Hill, *Chem. Lett.* **2014**, *43*, 36.
[61] J. Borges, J. F. Mano, *Chem. Rev.* **2014**.
[62] J. Hodak, R. Etchenique, E. J. Calvo, K. Singhal, P. N. Bartlett, *Langmuir* **1997**, *13*, 2708.
[63] E. A. Bayer, M. Wilchek, *Methods Enzymol.* **1990**, *184*, 138.
[64] O. Azzaroni, M. Álvarez, A. I. Abou-Kandil, B. Yameen, W. Knoll, *Adv. Funct. Mater.* **2008**, *18*, 3487.